Maps of the Cosmos
ASP Conference Series, Vol. 216, 2005
M. Colless, L. Staveley-Smith, R. Stathakis

Mapping the Reionization Era Through the 21 cm Line Emission

Benedetta Ciardi and Simon D. M. White
Max-Planck-Institut für Astrophysik, Karl-Schwarzschild-Str. 1, 85741 Garching, Germany

Abstract. We will present simulations of the IGM reionization process and discuss its observability through the 21 cm line. We find that the primordial stellar sources considered in this study give a value of the reionization epoch and of the electron optical depth consistent with the observations by *WMAP*, without invoking the presence of additional sources of ionization. Depending on the redshift of reionization, broad-beam observations at frequencies $< 100-150$ MHz with the next generation of radio telescopes should reveal angular fluctuations in the sky brightness temperature in the range $5-20$ mK on scales < 5 arcmin.

1. Introduction

Despite much recent theoretical and observational progress in our understanding of the formation of early cosmic structures and the high redshift universe, many fundamental questions remain only partially answered. When did the first luminous objects form, and what was their impact on the surrounding intergalactic gas? While the excess HI absorption measured in the spectra of $z \sim 6$ quasars in the SDSS has been interpreted as the signature of the trailing edge of the cosmic reionization epoch (e.g. Fan et al. 2002), the recent analysis of the first year data from the *WMAP* satellite infers a mean optical depth to Thomson scattering $\tau_e \sim 0.17$, suggesting that the universe was reionized at higher redshift (e.g. Kogut et al. 2003).

The study of intergalactic medium (IGM) reionization by primeval stellar sources has been tackled by several authors, both via semi-analytic and numerical approaches. Two main ingredients are required for a proper treatment of the reionization process: *i)* a model of galaxy formation and emission properties and *ii)* a reliable treatment of the radiative transfer of ionizing photons. Once a reionization history has been produced, different observational strategies can be proposed to test the model. It has long been known that neutral hydrogen in the IGM and gravitationally collapsed systems may be directly detectable in emission or absorption against the Cosmic Microwave Background radiation (CMB) at the frequency corresponding to the redshifted 21 cm line (see for example Tozzi et al. 2000; Carilli, Gnedin, & Owen 2002; Furlanetto & Loeb 2002; Iliev et al. 2003). Here, we discuss a model of the IGM reionization process and its observability through the 21 cm line emitted by neutral IGM.

https://doi.org/10.1017/S007418090019672X Published online by Cambridge University Press

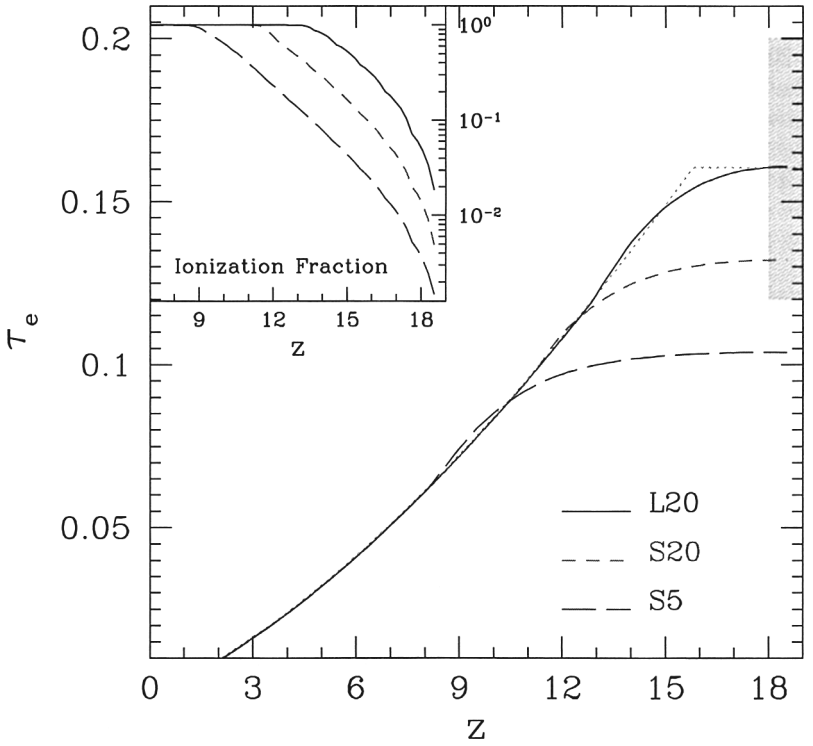

Figure 1. Redshift evolution of the electron optical depth, τ_e, for the S5 (long-dashed line), S20 (short-dashed) and L20 (solid) runs. The dotted line refers to sudden reionization at $z = 16$. The shaded region indicates the optical depth $\tau_e = 0.16 \pm 0.04$ (68% CL) implied by the Kogut et al. (2003) "model independent" analysis. In the inset the redshift evolution of the volume-averaged ionization fraction, x_v, is shown for the three runs.

2. Numerical Simulations of IGM Reionization

We have studied the galaxy formation and evolution process with a combination of high resolution N-body simulations and semi-analytic techniques (Ciardi, Ferrara, & White 2003; Ciardi, Stoehr, & White 2003). The simulations, based on a ΛCDM "concordance" cosmology, are run on a box of $20h^{-1}$ Mpc comoving side (the largest ever used to study the reionization process) representing a field region of the universe. The smallest resolved halos have masses of $M \simeq 10^9$ $M_\odot$ and start forming at $z \sim 20$. As for the galaxies emission properties, we have assumed a time-dependent spectrum of a simple stellar population of metal-free stars, with either a Salpeter or a mildly top-heavy (Larson) Initial Mass Function (IMF). Of the emitted ionizing photons, only a fraction f_{esc} will actually be able to escape into the IGM. This quantity is poorly determined both theoretically and observationally and may vary with, e.g., redshift, mass and structure of a galaxy, as well as with the ionizing photon production rate. Finally, the propagation into the given density field of the emitted ionizing photons is followed

https://doi.org/10.1017/S007418090019672X Published online by Cambridge University Press

with the radiative transfer code **CRASH** (Ciardi et al. 2001; Maselli, Ferrara, & Ciardi 2003).

The simulations of galaxy formation and reionization described above have been run for three different parameter combinations: Salpeter IMF and $f_{esc} = 5\%$ (S5); Salpeter IMF and $f_{esc} = 20\%$ (S20); Larson IMF and $f_{esc} = 20\%$ (L20). The critical parameter differentiating these runs is the number of ionizing photons escaping a galaxy into the IGM for each solar mass of long-lived stars which it forms. This number is maximized in the L20 run and minimized in the S5 one.

The redshift evolution of the volume-averaged ionization fraction, x_v, essentially coincident with mass-averaged one (Ciardi et al. 2003), is reported for each run in the inset of Figure 1. The three runs reach complete ionization ($x_v \approx 1$) at $z_r \approx 13$ (L20), 11 (S20) and 8 (S5). Finally, Figure 1 shows the evolution of τ_e corresponding to the above reionization histories, that we use to quantify the agreement between our simulations and the *WMAP* data ($\tau_e = 0.16 \pm 0.04$, 68% CL, implied by the Kogut et al. (2003) "model independent" analysis). The three runs yield the values $\tau_e = 0.104$ (S5), 0.132 (S20) and 0.161 (L20). A value $\tau_e = 0.16$ is also obtained if one assumes instantaneous reionization at $z_r \approx 16$ (dotted line).

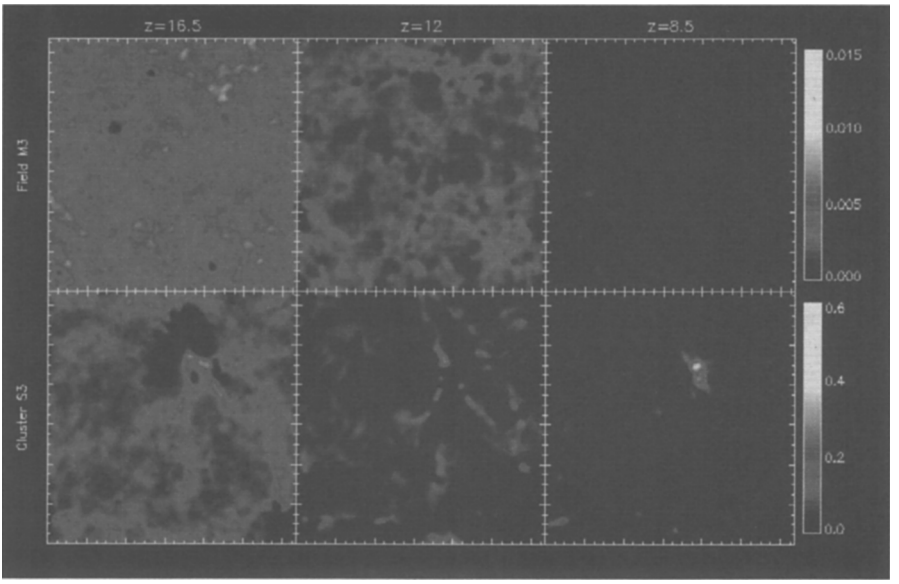

Figure 2. Slices through the simulation boxes (S5 runs). The six panels show the neutral hydrogen number density for the field region (upper panels) and the proto-cluster (lower panels), at redshift, from left to right, $z = 16.5, 12$ and 8.5.

To assess the impact of environment on the reionization process, an additional simulation has been run (with the same parameters of the S5 run) on a box of $10h^{-1}$ Mpc comoving side, centered on a proto-cluster (Ciardi et al. 2003). In Figure 2 we show illustrative slices cut through the simulation boxes.

https://doi.org/10.1017/S007418090019672X Published online by Cambridge University Press

The ionized regions (black) clearly grow differently in the two environments. In the field, high density peaks are uncommon and HII regions easily break into the IGM; in the proto-cluster the density is higher, so ionization is more difficult and recombination is faster. Moreover, many photons are initially needed to ionize the high density gas surrounding the sources, before photons can escape into the low density IGM. As a result, more photons are required to ionize the proto-cluster region, and filaments of neutral gas are still present after the field region is almost completely ionized.

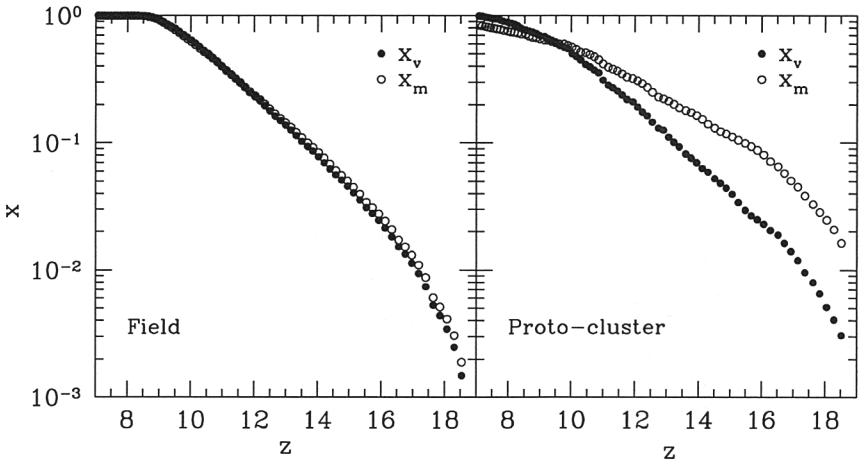

Figure 3. Redshift evolution of ionization fraction for the field region (left panel) and the proto-cluster (right panel) for the simulations in Figure 2. Volume (filled circles) and mass (open circles) averaged ionization fraction (x_v and x_m, respectively) are shown.

This is more clearly seen in Figure 3, where the redshift evolution of the volume (filled circles) and mass (open circles) averaged ionization fractions, x_v and x_m respectively, are compared both for the field region (left panel) and for the proto-cluster (right panel). The evolution proceeds differently in the two regions: initially the x_v are comparable, but the proto-cluster gas ionizes more slowly, for the reasons discussed above. The most interesting feature of these plots is that, while for the field region x_m is always comparable with x_v, $x_m > x_v$ initially in the proto-cluster, i.e. at first relatively dense cells are ionized. This because the density immediately surrounding the sources must be ionized, before the photons can break into the IGM. The trend reverses at later times, when large, low density regions get ionized and the highest density peaks remain neutral or recombine.

3. 21 cm Radiation Emission

The emission of the 21 cm line is governed by the spin temperature, T_S. In the presence of the CMB radiation, T_S quickly reaches thermal equilibrium with $T_{\rm CMB}$ and a mechanism is required that decouples the two temperatures. While

https://doi.org/10.1017/S007418090019672X Published online by Cambridge University Press

the spin-exchange collisions between hydrogen atoms proceed at a rate that is too small for realistic IGM densities, the Lyα pumping dominates, by mixing the hyperfine levels of neutral hydrogen in its ground state via intermediate transitions to the $2p$ state. At the epochs of interest, Lyα pumping will efficiently decouple T_S from $T_{\rm CMB}$ if $J_\alpha > 10^{-21}$ ergs cm^{-2} s^{-1} Hz^{-1} sr^{-1}. We find (Ciardi & Madau 2003) that the expected diffuse flux of Lyα photons should satisfy the above requirement during the 'grey age', from redshift ~ 20 to complete reionization. As the IGM can be easily preheated by primordial sources of radiation (e.g. Lyα and X-ray heating; Madau, Meiksin, & Rees 1997; Chen & Miralda-Escudé 2004), the universe will be observable in 21 cm emission at a level that is independent of the exact value of T_S. In Ciardi & Madau (2003) we have followed the emission produced by the reionization histories described above. Maps of antenna temperature can be directly derived from the maps of neutral hydrogen described in the previous Section. While the average 21 cm signal is two orders of magnitude lower than that of the CMB (and will be swamped by the much stronger non-thermal backgrounds that dominate the radio sky at meter wavelengths and that must be removed), its fluctuations – induced now both by inhomogeneities in the gas density and in the hydrogen ionized fraction – will greatly exceed those of the CMB. Brightness temperature fluctuations will be present both in frequency and in angle across the sky, and should be much easier to detect.

Figure 4 shows the expected rms temperature fluctuations relative to the mean, $\langle \delta T_b^2 \rangle^{1/2}$, produced by a gas volume (in our L20 reionization simulation) corresponding to a given bandwidth, $\Delta\nu = \nu_{obs}\Delta z/(1+z)$, and angular size $\Delta\theta$, as a function of $\Delta\theta$. The bandwidth is fixed for each redshift and equal to $\Delta\nu = 1$ MHz. The signal peaks at $z \sim 15$ (~ 90 MHz), corresponding to the epoch when several high density neutral regions are still present, but HII occupies roughly half of the volume. As the mass variance is larger on small scales, at a fixed bandwidth $\langle \delta T_b^2 \rangle^{1/2}$ increases with decreasing angular scale from about 5 to 20 mK. At lower redshift $\langle \delta T_b^2 \rangle^{1/2}$ decreases and it drops dramatically at $z < 13.5$, when the IGM gets close to complete reionization. Above redshift 15, the rms decreases again as the development of structures in the universe is less advanced. Although inhomogeneities in the ionized fraction drop to zero as the IGM is mostly neutral, a patchwork of radio emission is produced by regions with overdensities still in the linear regime and by voids. For the S5 reionization simulation, we obtain a similar behavior, except that now the neutral IGM is detectable up to frequencies of 150 MHz.

4. Summary

The main results of these studies can be summarized as follows.

i) Our field region of the universe gets reionized earlier than the proto-cluster, although the latter produces a higher number of ionizing photons. This is due to the fact that high density gas, which is more common in the proto-cluster, is more difficult to ionize and recombines much faster.

ii) While for the field region the mass and volume averaged ionization fractions, x_m and x_v respectively, are always comparable, x_m substantially exceeds x_v for the proto-cluster, at high redshifts. This is because the high density re-

https://doi.org/10.1017/S007418090019672X Published online by Cambridge University Press

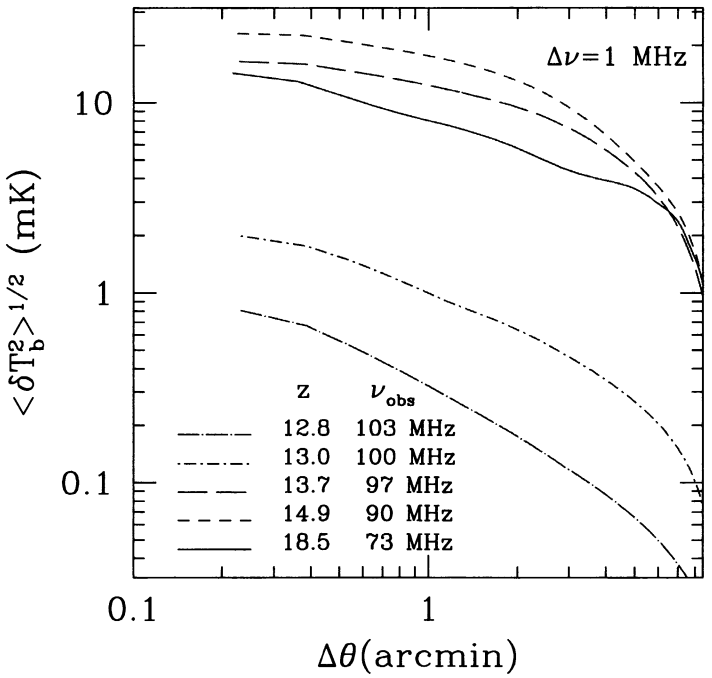

Figure 4. Expected rms brightness temperature fluctuations, $\langle \delta T_b^2 \rangle^{1/2}$, in our L20 simulation as a function of beam size $\Delta\theta$. A fixed bandwidth $\Delta\nu$ = 1 MHz has been assumed. Every curve corresponds to a different emission redshift or, equivalently, observed frequency ν_{obs}.

gions surrounding the sources have to be ionized first, before the photons can break out into the low density IGM.

iii) The primordial stellar sources considered in this study give a value of the reionization epoch and optical depth consistent with observations, without invoking the presence of additional sources of ionization.

iv) At epochs when the IGM is still mainly neutral, the simulated early galaxy population provides enough Lyα photons to decouple T_S from $T_{\rm CMB}$. As in the same redshift range the IGM is expected to be 'warm', the 21 cm line would be seen in emission.

v) The rms temperature fluctuations relative to the mean, increase with decreasing angular scale, as variance is larger on smaller scales. The signal peaks at an epoch when several high density neutral regions are still present, but HII occupies roughly half of the volume.

vi) Depending on the redshift of reionization breakthrough, broad-beam observations at frequencies $< 100 - 150$ MHz with the next generation of radio

https://doi.org/10.1017/S007418090019672X Published online by Cambridge University Press

telescopes should reveal angular fluctuations in the sky brightness temperature in the range $5 - 20$ mK (1σ) on scales < 5 arcmin.

Acknowledgments. We would like to thank our collaborators in the projects A. Ferrara, P. Madau and F. Stoehr.

References

Carilli, C., Gnedin, N. Y., & Owen, F. 2002, ApJ, 577, 22
Chen, X., & Miralda-Escudé, J. 2004, ApJ, 602, 1
Ciardi, B., Ferrara, A., Marri, S., & Raimondo, G. 2001, MNRAS, 324, 381
Ciardi, B., Ferrara, A., & White, S. D. M. 2003, MNRAS, 344, L7
Ciardi, B., & Madau, P. 2003, ApJ, 596, 1
Ciardi, B., Stoehr, F., & White, S. D. M. 2003, MNRAS, 343, 1101
Fan, X., et al. 2002, AJ, 123, 1247
Furlanetto, S., & Loeb, A. 2002, ApJ, 579, 1
Iliev, I. T., Scannapieco, E., Martel, H., & Shapiro, P. R. 2003, MNRAS, 341, 81
Kogut, A., et al. 2003, ApJS, 148, 161
Madau, P., Meiksin, A., & Rees, M. J. 1997, ApJ, 475, 492
Maselli, A., Ferrara, A., & Ciardi, B. 2003, MNRAS, 345, 379
Tozzi, P., Madau, P., Meiksin, A., & Rees, M. J. 2000, ApJ, 528, 597

https://doi.org/10.1017/S007418090019672X Published online by Cambridge University Press